Yu LING[1, 2], Guoxiang WU[1], Xu CAI[1]

Wind Power Research Centre, Shanghai Jiao Tong University (1), Department of Electrical Engineering, Shanxi Datong University (2)

Comparison of wind turbine efficiency in maximum power extraction of wind turbines with doubly fed induction generator

Abstract. *So far, much attention has been not received by the influence of the control modes on the wind turbine efficiency in maximum wind energy extraction, which is investigated based on variable speed wind turbines with doubly fed induction generator (DFIG) under vector control in stator flux orientation (SFO) in the paper. Prior art has tended to have an importance on investigating the principle and behaviors of control strategies in itself. As a result, two control modes, optimal rotor speed control mode and peak power control mode is investigated in detail. At first, Stator flux-orientated vector control for the rotor side converter of DFIG is reviewed, and in turn a comparison on two control modes is presented. Finally, a complete simulation model is developed to investigate how the operation of maximum wind energy extraction of the turbine below rated wind velocity, especially the wind turbine efficiency is affected by the two control methods. Simulation results are presented and compared under the two different control modes. Simulation results show that maximum wind energy extraction of the turbine and its efficiency is affected by different control modes.*

Streszczenie. *W artykule porównano różne strategie zarządzania systemem elektrowni wiatrowych z podwójnie zasilanym generatorem indukcyjnym. Jedna ze strategii polega na kontroli optymalnej prędkości wirnika, druga na kontroli mocy szczytowej. (**Porównanie wydajności turbiny wiatrowej przy strategii polegającej na otrzymaniu maksimum mocy**)*

Keywords: Vector control, Maximum wind power extraction, Wind generators, Wind turbine efficiency
Słowa kluczowe: wydajność turbiny wiatrowej, generator indukcyjny

1. Introduction

One of the main aims of wind turbine generation system development is to continuously improve wind turbine efficiency. The speed of the wind turbine determines the efficiency of the conversion of the energy in the wind into mechanical energy, for a given wind speed, blades geometry, and turbine orientation [1]. As a result, variable speed wind turbines, which can provide the capability of varying the turbine rotor speed according to wind speed, are now considered as an actual alternative to fixed speed wind turbines, and so variable speed wind turbines have better energy capture than fixed speed wind turbines [2]. Variable speed wind turbines can be divided into two broad subcategories depending on the VA rating of the power electronics employed in those systems. One is a synchronous or induction machine coupled to the grid through a power converter that has to be rated at 1 in p.u. total system power, and the losses of this converter is 3%. Another well-known configuration for variable speed wind turbines is the DFIG with a back-to-back voltage source converter between the grid and the rotor winding, and its stator winding can be connected directly to the grid, which is showed in Fig. 1. However this converter is typically 25% of total system power, and its losses only is 0.75% of total system power [3].

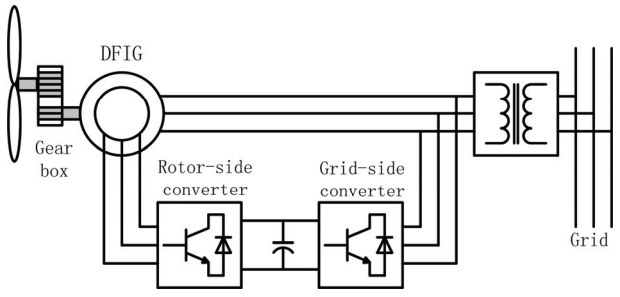

Fig.1. Schematic of DFIG wind power generation system

There are various types of control strategies that have been suggested for application in variable speed wind turbines with DFIG. Its aim is usually to maximize the output power, maximizing the efficiency of the energy conversion, maximizing the economic profit. Other objectives can be defined such as reducing mechanical stress and minimizing torque oscillations [1, 3]. In [4], the multi-scalar model of the double fed machine is presented, and the method is suitable for wind power generators. However, vector control of a doubly fed induction generator driven for variable speed wind turbine is becoming a popular alternative [2, 3, 5, 6]. Based on vector control methods, the usual strategy is to control the power or the torque acting on the wind turbine shafts [6]. An alternative control strategy has been presented in [7], where the rotational speed is the controlled variable.

However, the wind speed applied directly to the turbine blades is very hard and inaccurate to measure. Intelligent peak power tracking control techniques remove the speed measurement [8, 9], but it is usually slow in speed. In [10], a method of tracking the peak power is proposed in detail, which is independent of the turbine parameters and air density. The algorithm searches for the peak power by varying the speed in the desired direction. Direct power control for DFIG is a good alternative, too. The principles of this method are described in detail in [11, 12]. It is based on the measurement of active and reactive power on the grid side. The active and reactive powers are made to track references using hysteresis controllers. It offers several advantages such as eliminating complex coordinate transformation and the need for rotor position sensing. An improvement on the method is proposed in [13], and as a result several advantages such as no extra power or current control loops occur. But this is at the expense of a need for rotor position sensor.

There are many factors that influence the wind turbines efficiency, such as electrical characteristics of the generator, aerodynamic characteristics of the turbine blades and maximum power extraction control strategies [14]. In [15], two control methods of the DFIG, so called “direct” and “indirect”, have are studied and validated by simulation. Comparing with the indirect control, the direct control removes the current loop. But this could result in a high rotor current fluctuation.

However, the influence of control modes on wind turbine efficiency in maximum wind energy extraction has not received much attention so far. As a result, the paper focuses on the influence of control modes on wind turbine efficiency in maximum wind energy extraction under vector control in stator flux orientation based on variable speed wind turbines with DFIG. Two control modes, optimal rotor speed control mode, and peak power control mode is investigated in detail.

A complete simulation model including wind speed, wind turbine, generator and its control methods is developed for the control and test of maximum wind energy capturing and investigating how the wind turbine efficiency is affected by the two control methods.

2. Maximum Power Extraction Characteristics

The energy contained by the wind is in the form of kinetic energy. Its magnitude depends on the air density and the wind velocity. The wind power extracted by the turbine is given by the well-known expression [2]:

$$P_w = 0.5\rho S C_p(\lambda,\beta) v^3 \tag{1}$$

where P_w is the power extracted from the wind, ρ is the air density, S is the rotor swept area, v is the wind speed, C_p is the power coefficient, and λ is the tip speed ratio. The relationship between C_p, λ, and β depends on the blade design. However it can be reasonably approximated by the following equations [16]:

$$\begin{cases} C_p(\lambda,\beta) = 0.22\left(116/\lambda_i - 0.4\beta - 5.0\right)e^{-12.5/\lambda_i} \\ \dfrac{1}{\lambda_i} = \dfrac{1}{(\lambda + 0.08\beta)} - \dfrac{0.035}{(\beta^3+1)} \end{cases} \tag{2}$$

The tip speed ratio λ may be defined as the ratio of the turbine blade linear speed and the wind speed:

$$\lambda = 2\pi Rn/v = \omega_{wtr} R/v \tag{3}$$

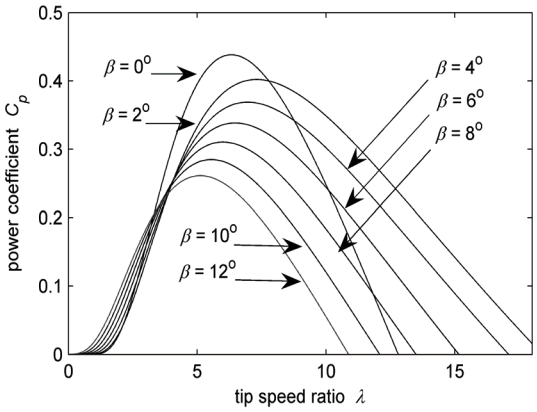

Fig. 2. Typical relationship between *Cp*, λ, and β

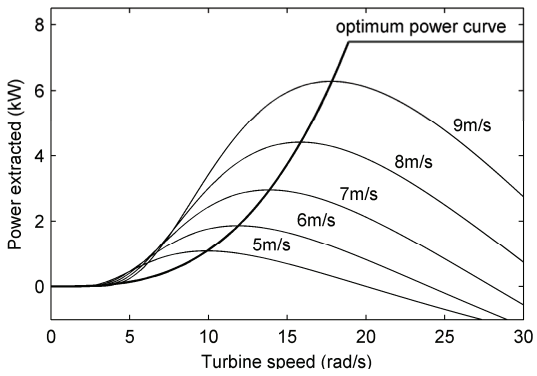

Fig. 3. Power and maximum power vs. wind turbine rotor speed

The C_p-λ characteristics, for different values of the pitch angle β, are illustrated in Fig. 2 based on (2). From above analysis, it can be found that there is a value of the tip speed ratio at which the power coefficient is maximal for the given wind speed (see Fig. 2), and the maximum achievable value of C_P, known as Betz limit, is $C_{P\max}$ = 0.593 [17]. The optimum power output curve for the wind turbine described in the Appendix is shown in Fig. 3. Variable speed turbines can be made to capture this peak energy in the wind by operating them at a blade speed that gives the optimum tip speed ratio or along the optimum power curve.

3. Wind Turbine Maximum Power Extraction Characteristics

In order to represent and test a variable-speed wind turbine with a DFIG in depth studies, mathematical models of the system have been developed in detail. These models include a representation of the wind, the turbine rotor and the drive train.

3.1 Wind Model

The variations of wind speed with time are predominantly random. In order to model a realistic wind characteristic, a random wind speed is used. The wind speed can vary between minimum and maximum values, characterizing a given site. It is calculated as an average value of the fixed-point wind speed over the whole rotor, and it takes the induction lag and the tower shadow into account [18]. A typical time evolution of the wind speed is represented in Fig. 4.

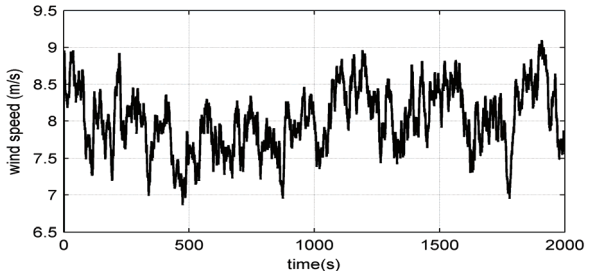

Fig. 4 A typical time evolution of the wind speed

3.2 Turbine Rotor Model

The aerodynamic model of the wind turbine rotor is based on the power coefficient C_P look-up table. The wind power is calculated by using the actuator disk theory. Assuming that the pitch angle β is constant we can rewrite the wind power developed by the turbine as following.

$$P_w = 0.5\rho S C_p(\lambda) v^3 \tag{4}$$

We know the equation for the wind turbine torque is:

$$T_m = P_w/\omega_{wtr} \tag{5}$$

where T_m is the wind turbine torque, ω_{tur} is wind turbine mechanical angular velocity.

3.3 Drive Train Model

The equivalent model of a wind turbine drive train is presented in Fig. 5 [19]. It is represented by a two masses model, with a flexible coupling between both of them which represents the gearbox. Noting that in the model we neglect the moment of inertia for the shafts and the gearbox wheels because they are small compared with the moment of inertia of the wind turbine or generator.

However in the paper a one-mass model is adapted. The equations of the model are:

$$T_{gen} - T_{wtre} = J_{ech}\frac{d\omega_{gen}}{dt} \tag{6}$$

$$J_{ech} = J_{gen} + J_{wtr}/k_{gear}^2 \tag{7}$$

$$T_{wtre} = T_{wtr}/k_{gear} \tag{8}$$

in these equations, all quantities are referred to the generator, and where J_{ech} denotes the equivalent moment of inertia; T_{wtre} is the equivalent wind turbine torque; T_{gen}, J_{gen} and

ω_{gen} are the generator torque, generator moment of inertia and generator mechanical speed, respectively; k_{gear} represents the gearbox ratio; J_{wtr} is the wind turbine moment of inertia.

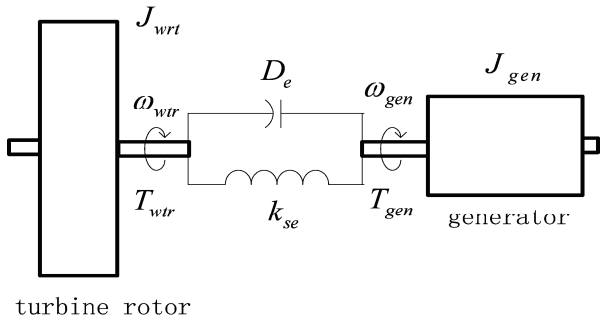

Fig. 5. Wind turbine drive train two-mass modeling on the generator side

And in Fig. 5, k_{se} is the equivalent spring constant, D_e denotes the equivalent mechanical damping coefficient.

4. DFIG Model and Its Control

As illustrated in Fig. 1, a DFIG is essentially a wound rotor induction machine with two power converter bridges connected back-to-back through an intermediate DC-voltage link between its rotor windings and the grid, and its stator windings can be connected directly to the grid. The objective of the grid-side converter control is to keep the dc link voltage constant and to tune the reactive power transfer between the generator rotor and the grid, while the rotor-side converter is responsible for control of the flux, and thus, the stator active and reactive power [2, 3].

The paper focuses on the rotor-side converter control for a DFIG, usually through a two-path controller consisting of a q-axis component controller and a d-axis component controller, in which the q-axis rotor current component is used for active power control, and the d-axis component is for reactive power control. The controller can operate in the stator-flux oriented reference frame in modern DFIG designs, and as a result it can be controlled independently through the decoupled d-q vector control approach [16].

The actual control signal of the rotor-side converter is shown in Fig. 6, where the d and q-axis reference voltages signal v_{rd_ref} and v_{rq_ref} to the three-phase sinusoidal control signal is illustrated. In the stator-flux-oriented frame, the v_α and v_β reference voltages can be obtained from the d and q-axis reference voltages through a vector rotation of $e^{j(\theta_s-\theta_r)}$, where θ_s and θ_r represent the stator flux position angle and the rotor position, respectively. The two α and β-axis voltages, together, are then used to generate the three-phase sinusoidal reference voltage signals, v_a, v_b, and v_c, for control of the rotor-side PWM converter [6], [20]. However, how to obtain the d and q-axis reference voltages v_{rd_ref} and v_{rq_ref}, and the stator-flux space vector position θ_s is investigated in detail that follows.

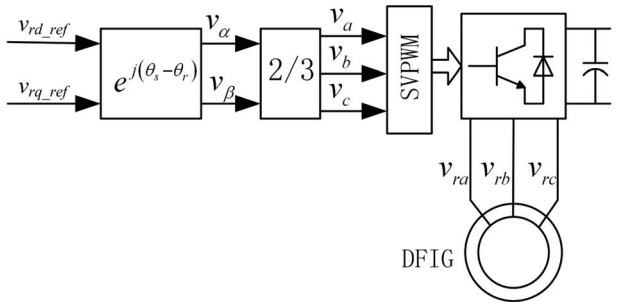

Fig. 6. Actual vector control for the DFIG

4.1 DFIG Model in the d-q Reference Frame

In term of the above analysis, the purpose of this section is to present the dynamic model of DFIG in d-q synchronous reference frame. For the simplicity, the rotor variables will be referred to the stator. It is assumed that magnetic circuit is linear. Using the motor convention, the stator and rotor voltages and fluxes in a d–q reference frame, rotating at synchronous angular electrical angular frequency ω_s in electrical angle, are given by [5]:

$$v_{sd} = R_S i_{sd} + \frac{d\psi_{sd}}{dt} - \omega_s \psi_{sq} \tag{9}$$

$$v_{sq} = R_S i_{sq} + \frac{d\psi_{sq}}{dt} + \omega_s \psi_{sd} \tag{10}$$

$$v_{rd} = R_r i_{rd} + \frac{d\psi_{rd}}{dt} - \omega_1 \psi_{rq} \tag{11}$$

$$v_{rq} = R_r i_{rq} + \frac{d\psi_{rq}}{dt} + \omega_1 \psi_{rd} \tag{12}$$

$$\psi_{sd} = L_s i_{sd} + L_m i_{rd} \tag{13}$$

$$\psi_{sq} = L_s i_{sq} + L_m i_{rq} \tag{14}$$

$$\psi_{rd} = L_r i_{rd} + L_m i_{sd} \tag{15}$$

$$\psi_{rq} = L_r i_{rq} + L_m i_{sq} \tag{16}$$

where v_{sd} and v_{sq} are the d- and q-axis stator voltages, and v_{rd} and v_{rq} are the d- and q-axis rotor voltages, respectively; i_{sd} and i_{sq} represent the d- and q-axis stator currents, and i_{rd} and i_{rq} represent the d- and q-axis rotor currents, respectively; R_s and R_r are the stator and rotor resistances per-phase, respectively. ω_1 is slip electrical angular frequency as the equation $\omega_1 = \omega_s - \omega_r$, in which ω_r is the rotor electrical angular velocity, and it is related to the rotational speed of the machine as the expression $\omega_1 = \omega_r / p$, where p is the pairs number of machine poles.

Also, ψ_{sd} and ψ_{sq} are the d- and q-axis stator flux, and ψ_{rd} and ψ_{rq} are the d- and q-axis rotor flux; L_s and L_r are the per-phase stator and rotor self-inductances, respectively, and L_m is the per-phase mutual inductance.

But the space vector approach is particularly useful in later analysis of stator flux vector oriented control. So the mathematical model of the DFIG using the space vector approach is necessary, and so (9) to (12) can be rewritten using the space vector approach as following [20]:

$$\bar{v}_{sdq} = R_S \bar{i}_{sdq} + \frac{d\bar{\psi}_{sdq}}{dt} - j\omega_s \bar{\psi}_{sdq} \tag{17}$$

$$\bar{v}_{rdq} = R_r \bar{i}_{sdq} + \frac{d\bar{\psi}_{rdq}}{dt} - j\omega_1 \bar{\psi}_{sdq} \tag{18}$$

where "¯" indicates an space vector.

Based on (17) and (18), the T-equivalent circuit of the doubly fed induction generator in d-q synchronous coordinates using the space vector approach is shown in Fig. 7.

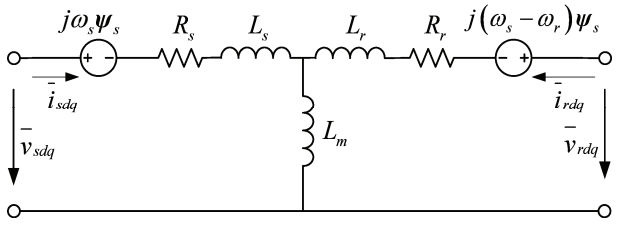

Fig. 7. T-equivalent of DFIG in the d-q synchronous reference frame

The generalized expression of the active and reactive

power in *d-q* synchronous reference frame is:

(19) $$P_s = 1.5\,\mathrm{Re}\left(\bar{v}_{sdq}\bar{i}^{*}_{sdq}\right) = 1.5\left(v_{sd}i_{sd} + v_{sq}i_{sq}\right)$$

(20) $$Q_s = 1.5\,\mathrm{Im}\left(\bar{v}_{sdq}\bar{i}^{*}_{sdq}\right) = 1.5\left(v_{sq}i_{sd} - v_{sd}i_{sq}\right)$$

And the electromagnetic torque is calculated by using the equation:

(21) $$T_e = -1.5\mathrm{p}\,\mathrm{Im}\left(\bar{\psi}_{sdq}\bar{i}^{*}_{sdq}\right) = 1.5\mathrm{p}\left(\psi_{sd}i_{sq} - \psi_{sq}i_{sd}\right)$$

where $\bar{i}^{*}_{sdq}$ is the conjugate of $\bar{i}_{sdq}$.

4.2 Stator-Flux Orientation Control for DFIG

The double fed induction generator is controlled in a synchronously rotating *d-q* axis reference frame, with the *d*-axis oriented along the stator-flux vector position. In this way, decoupled control between the electrical torque and the rotor excitation current is obtained.

Linking the synchronous reference frame to the stator flux as shown in Fig. 8, in which we can obtain:

(22) $$v_{sd} = 0$$

(23) $$\psi_{sq} = 0$$

Thus

(24) $$\left|\bar{v}_{sdq}\right| = \left|v_{sd} + jv_{sq}\right| = \left|0 + jv_{sq}\right| = v_{sq}$$

(25) $$\left|\bar{\psi}_{sdq}\right| = \left|\psi_{sd} + j\psi_{sq}\right| = \left|\psi_{sd} + j0\right| = \psi_{sd}$$

Based on (25), the relation of between stator fluxes and currents are given by the following simplifications below:

(26) $$\psi_{sd} = L_m i_{ms} = L_s i_{sd} + L_m i_{rd}$$

(27) $$0 = L_s i_{sq} + L_m i_{rq}$$

where i_{ms} is the stator magnetizing current.

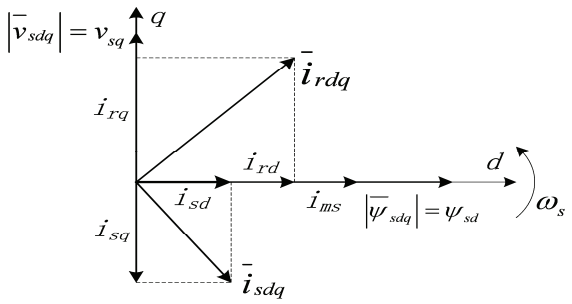

Fig. 8. Explicative to stator-flux oriented control

From (26) and (27), two orthogonal components of the stator current can be rewritten as following:

(28) $$i_{sd} = \left(i_{ms} - i_{rd}\right)L_m / L_s$$

(29) $$i_{sq} = -L_m i_{rq} / L_s$$

Substituting (15) and (16) in (11) and (12), respectively, and the rotor voltage equations can then be written as following:

(30) $$v_{rd} = R_r i_{rd} + L_r \frac{di_{rd}}{dt} + L_m \frac{di_{sd}}{dt} - \omega_1\left(L_r i_{rq} + L_m i_{sq}\right)$$

(31) $$v_{rq} = R_r i_{rq} + L_r \frac{di_{rq}}{dt} + L_m \frac{di_{sq}}{dt} + \omega_1\left(L_r i_{rd} + L_m i_{sd}\right)$$

And, in term of (28) and (29), the both equations above can be rewritten as:

(32) $$v_{rd} = R_r i_{rd} + \sigma L_r \frac{di_{rd}}{dt} + \frac{L_m^2}{L_s}\frac{di_{ms}}{dt} - \omega_1 \sigma L_r i_{rq}$$

(33) $$v_{rq} = R_r i_{rq} + \sigma L_r \frac{di_{rq}}{dt} + \omega_1 \frac{L_m^2}{L_s} i_{ms} + \omega_1 \sigma L_r i_{rd}$$

(34) $$\sigma = \left(1 - \frac{L_m^2}{L_s L_r}\right)$$

where σ is the T-equivalent inductance as seen from the rotor with the stator short-circuited, which can be saw in Fig.7 [5].

Rearranging (32) and (33), the below equations can be derived:

(35) $$v_{rd} = R_r i_{rd} + \sigma L_r \frac{di_{rd}}{dt} + E_d$$

(36) $$E_d = \frac{L_m^2}{L_s}\frac{di_{ms}}{dt} - \omega_1 \sigma L_r i_{rq}$$

(37) $$v_{rq} = R_r i_{rq} + \sigma L_r \frac{di_{rq}}{dt} + E_q$$

(38) $$E_q = \omega_1 i_{ms} L_m^2 / L_s + \omega_1 \sigma L_r i_{rd}$$

where E_d and E_q denotes the *d-q* rotor E.M.F voltage terms, respectively. In (36), the first term is the induced *d*-axis E.M.F term associated with the stator transients and the last term is the 'cross-coupling' induced *d*-axis E.M.F. term, while in (38), the first term is the induced *d*-axis E.M.F term associated with the stator stability and the last term is the 'cross-coupling' induced *q*-axis E.M.F. term.

The stator-flux position angle θ_s is calculated from its definition as following:

(39) $$\psi_{s\alpha} = \int\left(v_{s\alpha} - R_s i_{s\alpha}\right)dt$$

(40) $$\psi_{s\beta} = \int\left(v_{s\beta} - R_s i_{s\beta}\right)dt$$

(41) $$\theta_s = \tan^{-1}\left(\psi_{s\beta} / \psi_{s\alpha}\right)$$

where $v_{s\alpha}$ and $v_{s\beta}$ are the α- and β-axis stator voltages, $\psi_{s\alpha}$ and $\psi_{s\beta}$ are the α- and β-axis stator flux, $i_{s\alpha}$ and $i_{s\beta}$ represent the α- and β-axis stator currents, respectively.

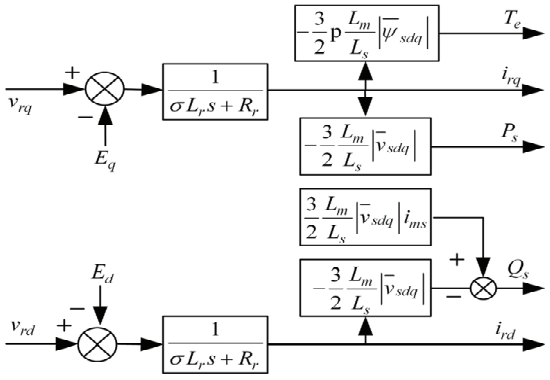

Fig. 9. Diagram of the DFIG

And in stator-flux orientation synchronously rotating *d-q* axis reference frame, and taking into account (28) and (29), the equations of stator active power, reactive power and the electromagnetic torque can be simplified, respectively:

(42) $$P_s = -\frac{3}{2}\frac{L_m}{L_s}\left|\bar{v}_{sdq}\right| i_{rq}$$

(43) $$Q_s = \frac{3}{2}\frac{L_m}{L_s}\left|\bar{v}_{sdq}\right|\left(i_{ms} - i_{rd}\right)$$

(44) $$T_e = -\frac{3}{2}\mathrm{p}\frac{L_m}{L_s}\left|\bar{\psi}_{sdq}\right| i_{rq}$$

The resulting bloc diagram of the DFIG is presented in Fig. 9.

4.3 Rotor Current Control Inner Loop

How to obtain the *d*- and *q*- axis reference voltages, v_{rd_ref} and v_{rq_ref}, is described in detail as following. In fact, this is the main objective of rotor current control inner loop.

In (32) and (33), the last term represents a cross-relation between the two current components. Since the stator is connected to the grid, and the influence of the stator resistance is small the stator flux is mainly determined by the stator voltage, it is practically constant. This implies that the derivative of the stator flux is close to zero and can be neglected. The generalized control law to obtain the desired currents can be described according to:

(45) $$v_{rd\_ref} = v_{rd} + \Delta v_{rd}$$

(46) $$v_{rq\_ref} = v_{rq} + \Delta v_{rq}$$

(47) $$v_{rd} = \left(k_{rp} + k_{ri}/s\right)\left(i_{rd\_ref} - i_{rd}\right)$$

(48) $$v_{rq} = \left(k_{rp} + k_{ri}/s\right)\left(i_{rq\_ref} - i_{rq}\right)$$

(49) $$\Delta v_{rd} = -\omega_1\left(L_r - L_m^2/L_s\right)i_{rq}$$

(50) $$\Delta v_{rq} = \omega_1\left(L_r - L_m^2/L_s\right)i_{rd} + \omega_1 i_{ms} L_m^2/L_s$$

where Δv_{rd}, Δv_{rq} are feed forward *d*- and *q*-axis voltage compensation terms, respectively; And k_{rp} and k_{ri} represent PI controller gains, respectively.

How to derive the *d*- and *q*-axis reference currents i_{rd_ref} and i_{rq_ref} are crucial. As a matter of fact, it is the outer control loop that is responsible for this. Generally, Outer control loop can be achieved by so-called 'speed control mode', 'power control mode', and 'torque control mode'. The first two control modes are the research interest of this paper.

4.4 Optimal Rotor Speed Control Mode

The method is based on regulating the velocity of the wind turbine, i.e., the controlled variable is the rotational speed of the turbine rotor. PI regulators with cascade control loops including inner current loop and outer speed loop control are used to control the *d-q* rotor-side converter currents and the windmill speed, as a result that it can realize the generator active and reactive power control. The generalized closed loop control strategy is shown in Fig. 10. ω_{rref} is the rotor speed command calculated as the optimal tip speed ratio λ_{opt}:

(51) $$\lambda_{opt} = k\omega_{r\_ref}/v$$

where v is wind speed, k is conversion coefficient, and it is assumed that λ_{opt} is a constant value, so maximal achievable power coefficient $C_{P\max}$ can be determined by λ_{opt} as (2), and as a result, power tracking is maximized.

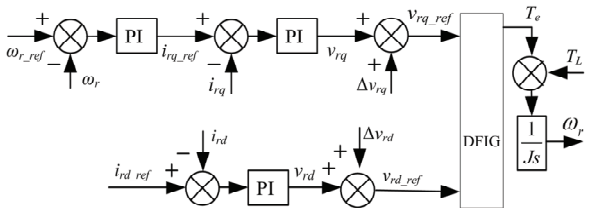

Fig. 10. Diagram of the optimum rotor speed control

The reference current i_{rq_ref} is derived from the error between the rotor speed command and the actual rotor speed by tuning a PI controller; the reference current i_{rd_ref} is calculated as (43) based on the reactive power, which can be set at any value, to produce or absorb reactive power from the grid, for considering power factor.

4.5 Peak power control method

The power control mode is based on regulating the active and reactive powers of the DFIG, i.e. the controlled variable is the power of the generator. The reference current i_{rq_ref} is derived from the error between the active power command and the actual active power by tuning a PI controller, and the reference current i_{rd_ref} is attained from the error between the reactive power command and the actual reactive power, as shown in Fig. 11, where the reactive power reference can be set at any value for considering power factor, and the active power reference P_{ref} can be calculated by the equation:

(52) $$P_{ref} = P_{\max}/\left(1-s\right) - P_{cus} - P_{Fe}$$

In term of (1) and (3), the extracted maximum wind power $P_{\max}$ is:

(53) $$P_{\max} = k_{\max}\omega_r^3$$

(54) $$k_{\max} = 0.5\rho S C_{p\max}\left(R/\lambda_{opt}\right)^3$$

where P_{cus} and P_{Fe} are copper losses and core losses, respectively, however, for simplicity, they are not considered in followed simulation study. s is the slip.

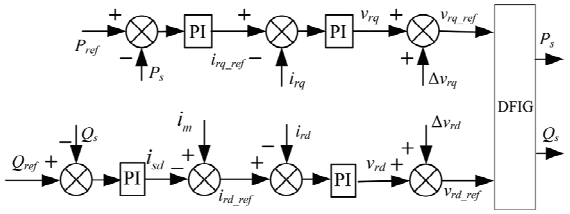

Fig. 11. Diagram of the optimum power control

5. Simulation evaluation and discussion

In the section, two maximum wind power extraction methods developed above are evaluated and compared through simulations in Matlab/Simulink. In order to compare the performance of the two control methods, the same wind speed data is adopted. Fig. 12 depicts the wind speed data used in the following simulations studies. The mean value of the wind speed is 8m/s. The initial rotor speed is set synchronous angular speed, and the wind turbine and DFIG parameters used in simulations are given in the Appendix.

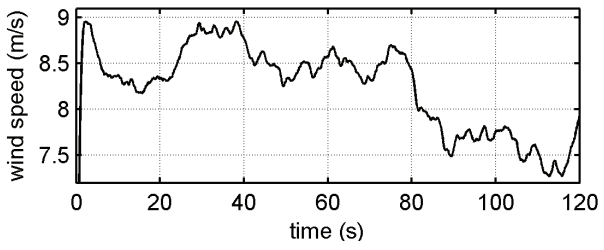

Fig. 12. Wind speed data used in the simulation studies

Fig. 13 shows the capability of maximum wind power extraction based on the optimal rotor speed control method. In Fig. 13(a), it is found that the turbine rotating speed can follow the reference speed smoothly as the wind speed varies. However, the maximum stator active power fluctuates sharply along the reference power that is calculated as (52), as shown in Fig. 13(b), and this result demonstrates the

capability of maximum wind power extraction under optimal rotor speed control, too.

Stator reactive power is shown in Fig. 13(c), where the reactive power reference is 0 Var. From Fig. 13(b) and Fig. 13(c), it is concluded that the decoupled control of active and reactive power can be realized.

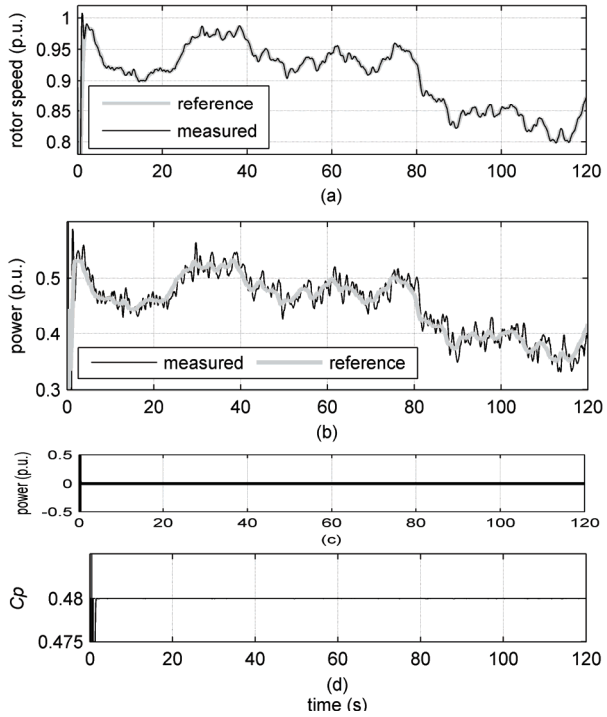

Fig. 13. Simulation result of the optimum rotor speed control

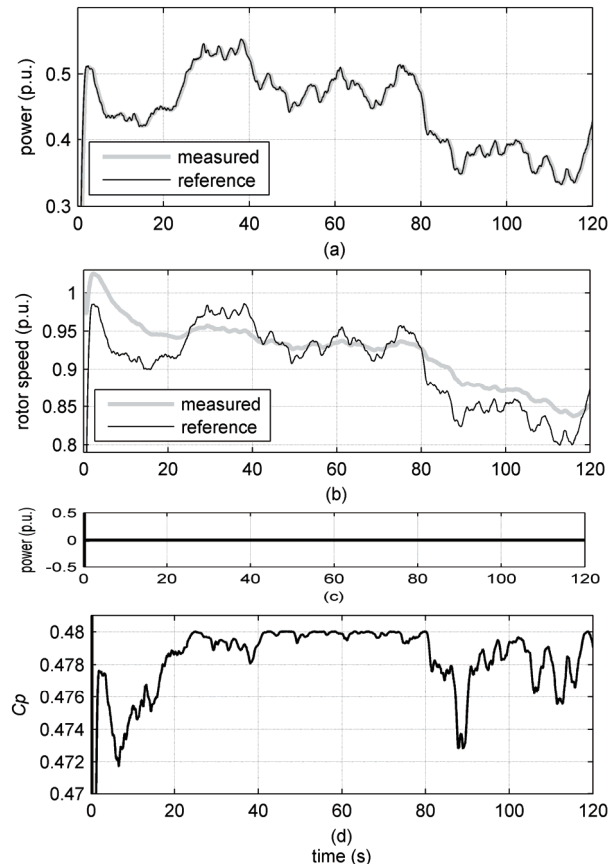

Fig. 14. Simulation result of the optimum power control

An almost constant $C_{P\max}$ is obtained, which can be saw in Fig. 13(d). And, this result also demonstrates that the rotational speed of the turbine rotor accurately follows the rotor speed reference ω_{r_ref}, which is calculated as (51) through the wind speed. As a result, a constant λ_{opt} can be derived.Fig. 14 shows the performance of the peak wind power tracking under peak power control mode. As shown in Fig. 14(a), the stator active power can track the power reference smoothly, while the sharp fluctuation of the stator active power can be seen in optimal rotor speed control mode.

It is noted that, however, the measured rotational speed of the turbine rotor cannot follow the rotor speed reference value, which is calculated as (51). As a result, this can result in a variable λ, and λ_{opt} cannot always be obtained. So, this can appropriately explain why a variable power coefficient C_p is obtained, as seen in Fig. 14(d).

Fig. 14(c) depicts stator reactive power, where reactive power reference is set 0 Var. From Fig. 14(a) and Fig. 14(c), it is found that the independent control of active and reactive power can be realized. The reactive power is determined by the desired power factor. Of course, this power is limited by the generator nominal power.

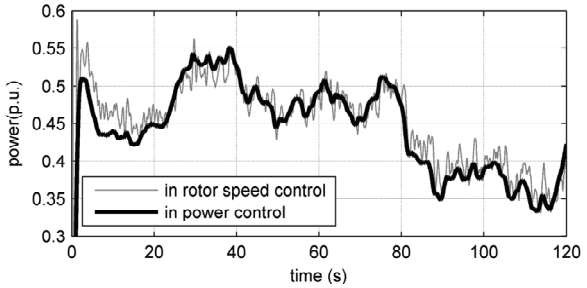

Fig. 15 a comparison on stator active power

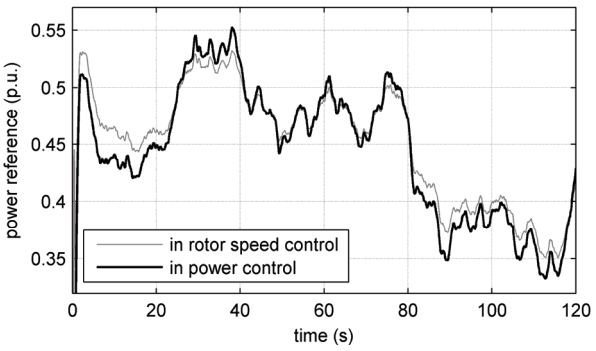

Fig. 16 a comparison on stator active power reference

Fig. 15 gives a comparison on stator active power between optimal rotor speed control mode and peak power control mode in steady-state operation. It is found that, though adopting the same wind speed data, the stator active power is different between the two control modes, i.e., the wind turbine efficiency is different between the two control modes. For the main, the wind turbine efficiency based on the optimal rotor speed control is larger than that using the peak power control modes. This result is also supported by Fig. 13(d) and Fig. 14(d). In Fig. 13(d), as above analysis, an almost constant maximum power coefficient $C_{P\max}$ is obtained, and as a result, the extracted maximum wind power $P_{\max}$ is obtained, while, as shown in Fig. 14(d), a variable power coefficient C_p is obtained, and as a consequence, $P_{\max}$ cannot always be obtained. As a fact, this result also can be appropriately explained by Fig. 16. As shown in Fig. 16, this is because the stator active power reference P_{ref}, which is

calculated as (52), is also different between the two control modes. As a matter of fact, the main reason is that the rotational speed cannot follow fast the reference rotor speed under peak power control, while the rotational speed can follow fast the reference rotor speed under optimal rotor speed control.

6. Conclusion

A comparative study of the control of maximum wind energy extracting in variable speed wind turbine with DFIG has been proposed. Two control modes including optimal rotor speed control mode and peak power control mode has been presented and the wind turbine efficiency is compared between the two control modes.

All of two control modes can provide the capability of independent control of active and reactive power, and realize the maximum power extraction of the turbine, which is consistent with that reported in other literatures [2], [6].

It is also found that stator active power fluctuates sharply in the rotor speed control mode, while in the power control mode, active power shift smoothly.

However, it is worth noting that, for the main, the wind turbine efficiency based on the optimal rotor speed control is larger than that using the peak power control modes under the same wind speed data condition. However, the improvement of wind turbine efficiency in optimal rotor speed control also depends on the accurate, fast, and real-time measurement of wind speed.

So it is very important to investigate how to measure accurately wind speed in optimal rotor speed control and how to attain fast rotor speed response characteristic in peak power control.

Appendix

DFIG Parameters:

P_s = 7.5kW, V_n = 220V, f = 50Hz, R_s = 0.2943Ω, L_s = 0.03651H, R_r = 0.1442Ω, L_r = 0.03573H, L_m = 0.03517H, Pairs number of pole = 3, Rated speed = 970rpm, J_{gen} = 0.472kgm^2

Wind Turbine Parameters:

Rotor radius = 3.2m, Air density = 1.225kg/ m^3, J_{wtr} = 7.5 kgm^2, k_{gear} = 5.065

Acknowledgements

This work was supported by Fund of Shanghai Science and Technology Commission (No.10dz1203902).

REFERENCES

[1] Rubira S.D., McCulloch M.D., Control Method Comparison of Doubly Fed Wind Generators Connected to the Grid by Asymmetric Transmission Lines, *IEEE Trans. industry applications*, 36(2000), No. 5, 986–991

[2] Chowdhury B.H., Chellapilla S., Double-fed induction generator control for variable speed wind power generation, *Electric Power System Research*, 76(2006), No. 9-10, 786–800

[3] Muller S., Deicke M., Doncker R.W.D., Doubly fed induction generator systems for wind turbines, *IEEE Ind. Applicat. Mag.*, 8(2002), No 3, 26–33

[4] Krzeminski Z., Sensorless multiscalar control of double fed machine for wind power generators, *The IEEE Conference on POWER CONVERSION*, April 2-5, 2002, Osaka, Janpan.

[5] Chondrogiannis S., Barnes M., Stability of doubly-fed induction generator under stator voltage orientated vector control, *IET Renew. Power Gener.*, 2(2008), No. 3, 170–180

[6] Pena R., Clare J.C., Asher G.M., Doubly fed induction generation using back-to-back PWM converters and its application to variable speed wind-energy generation, *IEE Proc.-Electr. Power Appl.*, 143(1996), No. 3, 231–241

[7] Mihet-Popa L., Blaabjerg F., Boldea I., Wind turbine generator modeling and simulation where rotational speed is the controlled variable, *IEEE Trans. Ind. Appl.*, 40(2004), No.1, 3–10

[8] Calderaro V., Galdi V., Piccolo A., Siano P., A fuzzy controller for maximum energy extraction from variable speed wind power generation systems, *Electric Power Systems Research*, 78(2008), No. 6, 1109–1118

[9] Wang Q., Chang L., An intelligent maximum power extraction algorithm for inverter based variable speed wind turbine systems, *IEEE Trans. Power Electron.*, 19(2004), No. 5, 1242–1249

[10] Datta R., Ranganathan V.T., A method of tracking the peak power points for a variable speed wind energy conversion system, *IEEE Trans. Energy Convers.*, 18(2003), No. 1, 163–168

[11] Xu L., Cartwright P., Direct active and reactive power control of DFIG for wind energy generation, *IEEE Trans. Power Electron*, 21(2006), No. 3, 750–758

[12] Datta R., Ranganathan V.T., Direct power control of grid-connected wound rotor induction machine without rotor position sensors, *IEEE Transactions on Power Electronics*, 16(2001), No. 3, 390-399

[13] Zhi D., Xu L., Direct power control of DFIG with constant switching frequency and improved transient performance, *IEEE Trans. Power Electron.*, 22(2007), No. 1, 110–118

[14] Li S., Haskew T.A., Muljadi E., Doubly fed induction generator maximum wind power extraction study through integrated steady-state and closed-loop control evaluation, *Electric Power Components and Systems*, 38(2010), No. 7, 767–785

[15] Boyette A., Saadate S., Poure P., Direct and indirect control of a doubly fed induction generator wind turbine including a storage unit, *The 32nd Annual IEEE Conference on INDUSTRIAL ELECTRONIC*, November 7-10, 2006, Paris, France.

[16] Yang S.Y., Zhang X., Zhang C.W., Chang L., Development of a variable-speed wind energy conversion system based on doubly-fed induction generator, *The 22nd Annual IEEE Conference and Exposition on APPLIED POWER ELECTRONICS*, February 25 -March 1, 2007, New York, USA.

[17] Bianchi F.D., Battista H.D., Mantz R.J., *Wind Turbine Control Systems: Principles, Modeling and Gain Scheduling Design*, (London: Springer-Verlag, 2007, 10–16)

[18] Vihriala H., *Control of variable speed wind turbines*, PhD dissertation, Dept. Elect. Eng., Tampere University of Technology, Findland, 2002

[19] Iov F., Daniela A., Sorensen H.P., *Wind Turbine Blockset in Matlab/Simulink: General Overview and Description of the Models*, (Aalborg: UNI. PRINT Aalborg University, 2004, 26-28)

[20] Li S., Haskew T.A., Characteristic study of vector-controlled doubly-fed induction generator in stator-flux-oriented frame, *Electric Power Components and Systems*, 36(2008), No. 9, 990–1015

Authors: *Yu LING. (1) 800 Dongchuan Road, Mulan Biulding B111, Shanghai, 200240, China; (2) 52 Pingquan Road, Kuang District, Datong, Shanxi, 037003, China. E-mail: pleasurely@126.com; Guoxiang WU, Xu CAI. 800 Dongchuan Road, Mulan Biulding B111, Shanghai, 200240, China. E-mail: wuguoxiang@ntu.edu.cn, caixu_cumt@263.net.*